ARTICLE

Tuning Structural, Electronic, and Magnetic Properties of Black-AsP Monolayer by Adatom Adsorptions: A First Principles Study

Xin Liu, Yu-xiang Ni, Hong-yan Wang, Hui Wang*

School of Physical Science and Technology, Key Laboratory of Advanced Technologies of Materials, Ministry of Education of China, Southwest Jiaotong University, Chengdu 611756, China

(Dated: Received on July 10, 2019; Accepted on October 6, 2019)

Black Arsenic-phosphorus (AsP) monolayer is a novel two-dimensional nanomaterial with the characteristics of modest direct bandgap and superhigh carrier mobility. However, little is known about how the surface adsorption affects the property of AsP monolayer. Motivated by this, we researched systematically the geometry, adsorption energy, magnetic moment and electronic structure of 11 different adatoms adsorbed on AsP monolayer using first-principles calculations. The adatoms used in this study include light nonmetallic (C, N, O) adatoms, period-3 metal (Na, Mg, Al) adatoms, and transition-metal (Ti, V, Cr, Mn, and Fe) adatoms. The adatoms cause an abundant variety of structural, magnetic and electronic properties. This study shows that AsP binds strongly with all adatoms under study and the adsorption energies in all systems are much stronger than that on graphene, SiC, BN, or MoS_2. The semiconductor property of AsP is affected by the introduction of adsorbed atoms, which can induce mid-gap states or cause n-type doping. Moreover, the adatom adsorptions cause various spintronic characteristics: N-, Ti-, and Fe-adsorbed AsP become bipolar semiconductors, while the Mn-decorated AsP becomes a bipolar spin-gapless semiconductor. Our results suggest that atomic adsorption on AsP monolayers has potential application in the field of nanoelectronics and spintronics.

Key words: AsP monolayer, Adsorption, Magnetism, Electronic property, Spin polarization

I. INTRODUCTION

Since graphene is discovered in 2004 [1], two dimensional (2D) layer materials such as h-BN [2, 3] and transition metal dichalcogenides [4, 5] have attracted great interest because of their particular structure, novel electronic properties, rich physics, and potential applications. However, there are many different kinds of inherent weakness in these materials. For instance, the electronic structure of graphene presents a zero bandgap which limits its application in semiconductor. MoS_2 has a relatively low mobility which impedes its use in electronic devices. This further stimulates the motivation to pursue more novel two-dimensional materials with better performance. In recent years, single-layer phosphorene, a new 2D nanomaterial has been fabricated [6–9]. Phosphorene has a variety of excellent properties, such as a modest direct bandgap semiconducting nature [10], high carrier mobilities ($300-1000\ cm^2{\cdot}V^{-1}{\cdot}s^{-1}$) [11, 12], and characteristic thermoelectric performance [13–15]. These properties make phosphorene be a material with multiple potential applications, including field-effect transistors [16–21], Li- and Na-ion batteries [22–24], spintronics [25], supercapacitors [26], and gas sensors [27–29]. With further research, a novel phosphorene-like material, arsenic phosphide (AsP) monolayer is discovered by a new synthetic approach adopting the alloying strategy [30]. The bandgap of AsP monolayer can be adjusted by the chemical compositions (As_xP_{1-x} with x in the range of $0-0.83$) [31]. $As_{0.5}P_{0.5}$ monolayer has a modest direct bandgap, and a high carrier mobility of $\sim$14380 $cm^2{\cdot}V^{-1}{\cdot}s^{-1}$ [32, 33], which makes it be an electron donor materials in excitonic solar cells. This fully shows that AsP monolayer has broad prospects in the application of photovoltaic devices.

For 2D materials, the defects and impurities which are introduced in the exfoliation or growth processes, can observably change the thermal, electronic, and mechanical properties. As a result, intentional introduction of specific defects should be a feasible way to change the features of the initial material. In a previous report, vacancies are observed in phosphorene by scanning tunneling microscopy (STM) [34]. The defect-induced states can also serve as scattering centers, which affect the transport properties of 2D materials. Surface adsorption is another possible approach of chemical functionalization of nanomaterials. Atomic

*Author to whom correspondence should be addressed.
E-mail: wanghui@swjtu.edu.cn

adsorption on 2D materials results in versatile structural, magnetic and electronic properties. For instance, the adsorption of transition-metal (TM) atoms on graphene remarkably introduces magnetism into the electronic structure of graphenes [35], while light nonmetallic adatoms can increase the bandgap of graphene with various p- or n-type doping features [36]. Similar phenomena have already appeared in germanene and silicene [37–42].

So far, little is known about how the surface adsorption affects the property of AsP monolayer. Motivated by this, we researched synthetically the structural, electronic and magnetic properties of 11 kinds of adatom adsorbed on AsP monolayer. The 11 different adatoms include light nonmetallic (C, N, O) adatoms, period-3 metal (Na, Mg, Al) adatoms, and transition-metal (Ti−Fe) adatoms. By using first principles calculations, in this work, we investigated the influence of adatoms on the geometry, adsorption energy, charge density difference, band structure, magnetic moment, and electronic density of states (DOS) of single-layer AsP. It is noteworthy that the adsorption of adatoms causes diverse structural, electronic and magnetic properties. The results of our research should be useful in fundamental studies of AsP monolayer, and they can also expand its potential application in many significant fields. For example, adsorption of N and O on single-layer AsP can reveal its surface reactivity and then reflect whether AsP can exist stably in the air. The reaction with Na atom is related with the potential application of AsP in Na-ion battery.

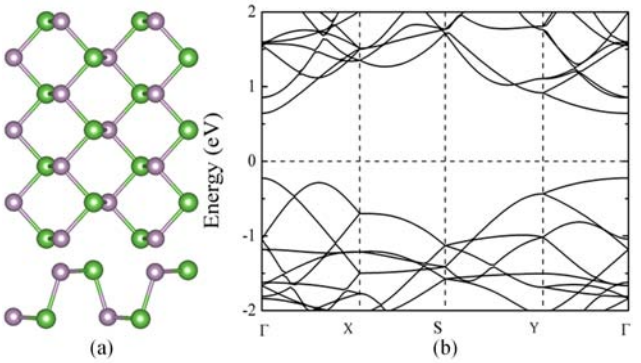

FIG. 1 (a) Illustration of top and side view of AsP monolayer. (b) Electronic band structure of pristine AsP.

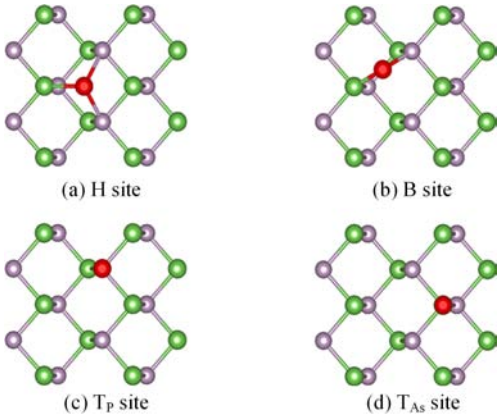

FIG. 2 Typical adatom adsorption sites on AsP monolayer: (a) H, (b) B, (c) T_P, and (d) T_{As}.

II. THEORETICAL METHODS

Our studies are performed by using first-principles method within spin-polarized density functional theory (DFT), as implemented in the Vienna *ab initio* simulation package (VASP) code [43, 44]. Generalized gradient approximation (GGA) in combination with Perdew-Burke-Ernzerhof (PBE) function is used to describe the exchange-correlation interaction [45]. Ion cores are described by projector augmented wave (PAW) potentials [46]. The Grimme's DFT-D2 approach is used to further describe van der Waals (vdW) interactions [47]. A plane-wave basis set with a maximum plane-wave energy of 550 eV is used for the valence electron wave functions. Gaussian smearing with a width of δ=0.05 eV is used for the occupation of the electronic levels, the Brillouin zone is sampled with a 7×7×1 Γ-centered k-point grid for structure optimization, and a more dense 17×17×1 Γ-centered k-point grid is used for electronic structure calculations. The optimized structures are obtained by relaxing all atomic positions using the conjugate gradient algorithm until all forces are smaller than 0.005 eV/Å, when the convergence of electronic self-consistent energy is less than 1.0×10^{-5} eV. Periodic boundary condition and vacuum space of ∼20 Å along z-directions are set in order to avoid interactions between two layers.

To simulate the adsorption of isolated atoms, a 2×3 supercell of AsP monolayer is selected. The optimized geometry of AsP monolayer is illustrated in FIG. 1(a). The calculated lattice parameters for AsP monolayer are a=4.60 Å and b=3.51 Å, which are highly consistent with the previous theoretical results [30, 32, 33].

The calculated band structure of AsP monolayer is illustrated in FIG. 1(b). Both the valence band maximum (VBM) and conduction band minimum (CBM) are located at the Γ point with a band gap of 0.86 eV, showing a direct bandgap in this system.

The adsorption energy (E_{ad}) of adsorption systems is defined as

$$E_{ad} = E_{A+AsP} - E_A - E_{AsP} \quad (1)$$

where E_{A+AsP}, E_A, and E_{AsP} are the total energies of AsP with adatom, the single adatom, and pristine AsP, respectively. As illustrated in FIG. 2, there are four highly symmetric adsorption positions for adatom: the H site at the center of the AsP hexagon, the B site above the middle-point of the lower P−As bond, the T_P site on the top of the upper P atom, and the T_{As} site on the

DOI:10.1063/1674-0068/cjcp1907136

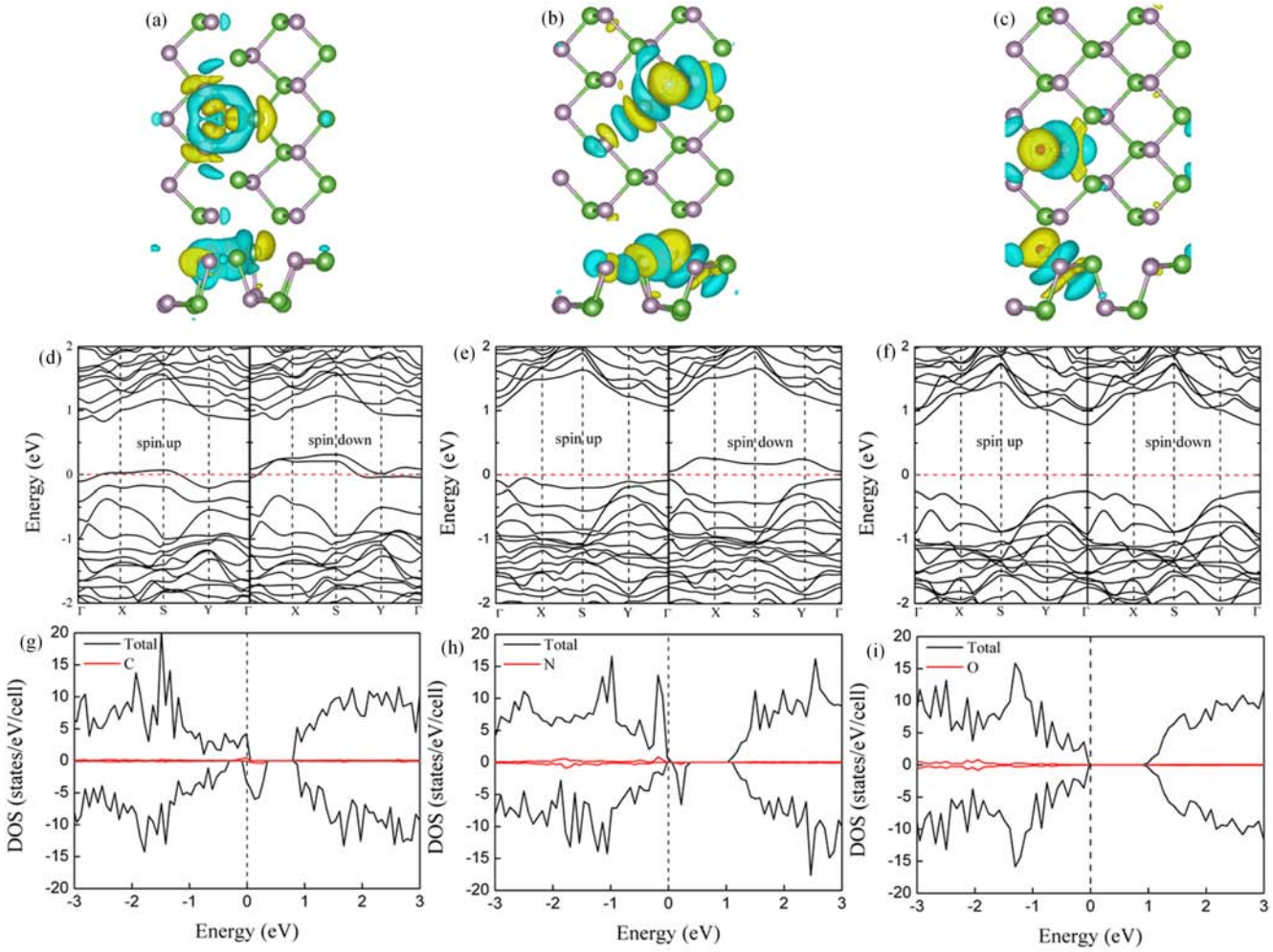

FIG. 3 The charge density difference of single (a) C, (b) N, and (c) O adsorbed on the AsP monolayer; the band structure of (d) C-, (e) N-, and (f) O-adsorbed AsP; the PDOS of (g) C-, (h) N-, and (i) O-adsorbed AsP.

top of the upper As atom. The negative value of $E_{\rm ad}$ reveals that the calculated adatom-AsP system is stable and the absolute value of $E_{\rm ad}$ indicates the strength of the interaction between AsP and the adatoms.

III. RESULTS AND DISCUSSION

A. Light nonmetallic (C, N, O) adatoms

First, we research the adsorptions of C, N and O atoms on AsP monolayer. These adatoms produce various adsorption structures on AsP, as shown in FIG. 3. The C adatom pushes As atom away from its primitive position and holds the H site with an adsorption energy ($E_{\rm ad}$) of −4.92 eV, while N adatom favors the B site and its adsorption energy ($E_{\rm ad}$) is −3.71 eV. The O adatom prefers the T_p site with the adsorption energy ($E_{\rm ad}$) of −5.75 eV. The C adatom is embedded in the AsP monolayer plane, however the N and O adatoms are adsorbed at the top of the plane, and C, N, and O adatoms form bond(s) with three, two, and one atom(s) of AsP monolayer, respectively.

In order to make sense of the charges redistribution of the decorated system, the charge density difference is calculated. When C atom is adsorbed on AsP, these sp^2-like bonds are almost on the same plane, in which the charge density accumulates in region of adatom and P(As). The electronegativity of C atom is nearly equal to that of P atom, then it destroies the original sp^3 bonds of the pristine AsP, and forms new sp^2 bonds with the P(As) atoms. N and O adatoms combined with two or one P(As) atom(s). The increase of the charge density around the adatom shows that N and O adatoms obtain electrons from atoms (P or As) of the AsP monolayer. Since the electronegativities of N and O atoms are stronger than that of P(As) atoms, electrons are attracted to these adatoms from the P(As) atoms. It is worth noting that O atom with s^2p^4 configuration obtains the lone pair from P atom, forming a bond with a bond length of 1.52 Å. The bond length is much shorter than the sum of the P (1.07 Å) and

DOI:10.1063/1674-0068/cjcp1907136

O (0.66 Å) covalent radii [48], which indicates a P=O double bond. Furthermore, the bond length in O−AsP system is in good agreement with the P=O double bond length of 1.51 Å in phosphoric acid [49]. Judging from the number of bonding atoms, the adsorption energies are supposed to follow the order of C>N>O. However, because of the formation of P=O double bond, the adsorption energy of O−AsP system increases greatly, the order of adsorption energy is changed to O>C>N.

FIG. 3 depicts the band structures and the density of states (DOS) of C, N, and O adsorption on AsP monolayer. The spin polarized band structures appeared in C and N adsorbed systems. The total magnetic moments of C and N adsorption on AsP are 1.37 μ_B and 0.99 μ_B, respectively. We think that the magnetism is mainly from the distorted P(As) atoms surrounding the adatom. For the C-adsorbed AsP, the defect state crosses the Fermi level, resulting in a metallic behavior. For the N adsorbed AsP, mid-gap down-spin state apears near the Fermi level and the bandgap is reduced to 0.12 eV. The adsorption of O atom causes several small peaks in the deep of valence bands between −3 and −2 eV, as illustrated in FIG. 3(i). Therefore, the O-adatom does not lead to any spin-polarized states, even though it merely widens the bandgap by 0.18 eV. This suggests that O atom do not change magnetic propertiy of AsP.

TABLE I Calculated structural and magnetic properties for single atoms adsorbed on (2×3 supercell) AsP at the most favorable adsorption sites.

Adatom	Site	E_{ad}/eV	μ/μ_B	ΔQ/e	d/Å
C	H	−4.92	1.37	−1.47	1.77 (A−P)
N	B	−3.71	0.99	−1.54	1.60 (A−P)
O	T_P	−5.75	NM	−1.32	1.52 (A−P)
Na	H	−1.57	NM	0.80	2.89 (A−P)
Mg	H	−0.94	NM	0.83	2.81 (A−As)
Al	H	−2.33	NM	0.91	2.59 (A−P)
Ti	H	−3.70	2.00	0.97	2.44 (A−P)
V	H	−3.11	4.07	0.79	2.36 (A−P)
Cr	H	−1.95	4.98	0.67	2.42 (A−P)
Mn	H	−2.04	4.99	0.56	2.43 (A−P)
Fe	H	−3.14	2.00	0.36	2.22 (A−P)

E_{ad}: adsorption energies; μ: the net magnetic moments, where NM refers to non-magnetic system; ΔQ: Bader charge transferred from adatom to AsP; d: minimum adatom-AsP (A−P or A−As) distances.

B. Period-3 metal (Na, Mg, Al) adatoms

Next, we considered the adsorption of period-3 metal atoms (Na, Mg, Al) on the AsP monolayer. The corresponding adsorption energies and geometrical parameters are shown in Table I. Through full geometry optimization, all of these adatoms favor the H site of AsP. Such a phenomenon is representative for the metal adsorbates, which generally favors high coordination adsorption sites on materials surfaces. The adsorption energies (E_{ad}) are 1.57 eV, 0.94 eV, and 2.33 eV for Na, Mg, and Al adatoms, respectively. The shortest bond length is 2.89 Å, 2.81 Å, and 2.59 Å for Na, Mg and Al adatoms, and the Bader charge analysis displays that 0.80 |e| , 0.83 |e|, and 0.91 |e| is transferred from Na, Mg, and Al to AsP, respectively. If the adsorption energy strength is analyzed only from bond length and charge transfer, the result is inconsistent with the calculation result. In order to further analyze the adsorption energy, we studied the charge density difference for Na, Mg, and Al adatoms adsorbed on AsP monolayer, as shown in FIG. 4. For Na and Mg (FIG. 4 (a) and (b)), the charge is mainly transferred from the adatoms to P(As) to form ionic bonds. At the same time, it can be seen that Na adatom has relatively strong interaction with four atoms of AsP monolayer, while Mg atoms interact strongly with only three atoms. FIG. 4(c) depicts that there is remarkably charge accumulation between the Al and P(As) atoms, which suggests the covalent bonding feature of the Al-AsP system. Therefore, the adsorption energy should follow the order of Al>Na>Mg, which is consistent with the calculated results. The adsorption energy of Na atoms adsorption on AsP is greater than that on graphene, which is also an advantage of AsP over graphene. The Na-graphene adsorption energy is smaller than the experimental cohesive energy per atom of the bulk Na metal. The battery performance can be improved by introducing edges, defects, or nitrogen/boron doping in graphene [50–52]. On the contrary, Na atom can easily bind to single-layer AsP without any doping/defect treatment. The adsorption energy of Na-AsP system is larger than its bulk cohesive energy, indicating that Na atoms are more likely to form a two-dimensional layered structure on the AsP than clustering together. Then single-layer AsP is an extremely promising anode material for sodium ion batteries.

To illustrate the electronic structure of metal (Na, Mg, Al) adatoms adsorbed AsP monolayer, the band structures and the total and projected densities of states (DOS) are also presented in FIG. 4. All of these adsorptions do not cause any magnetic changes. As a result of Na and Al adatoms adsorption, the semi-conductive AsP becomes metallic, while the Mg adsorption maintains the semiconductor property of AsP. The adsorption of Na atom does not substantially change the entire DOS of the AsP, however it just moves the Fermi level into conduction bands, causing an n-type doping in AsP. Mg adatom brings mid-gap defect states into AsP, which cuts down the bandgap to 0.49 eV. The Al 3p orbits induce several small defect peaks between 0 and −1.5 eV in the DOS and cause the conduction band through the Fermi level.

DOI:10.1063/1674-0068/cjcp1907136

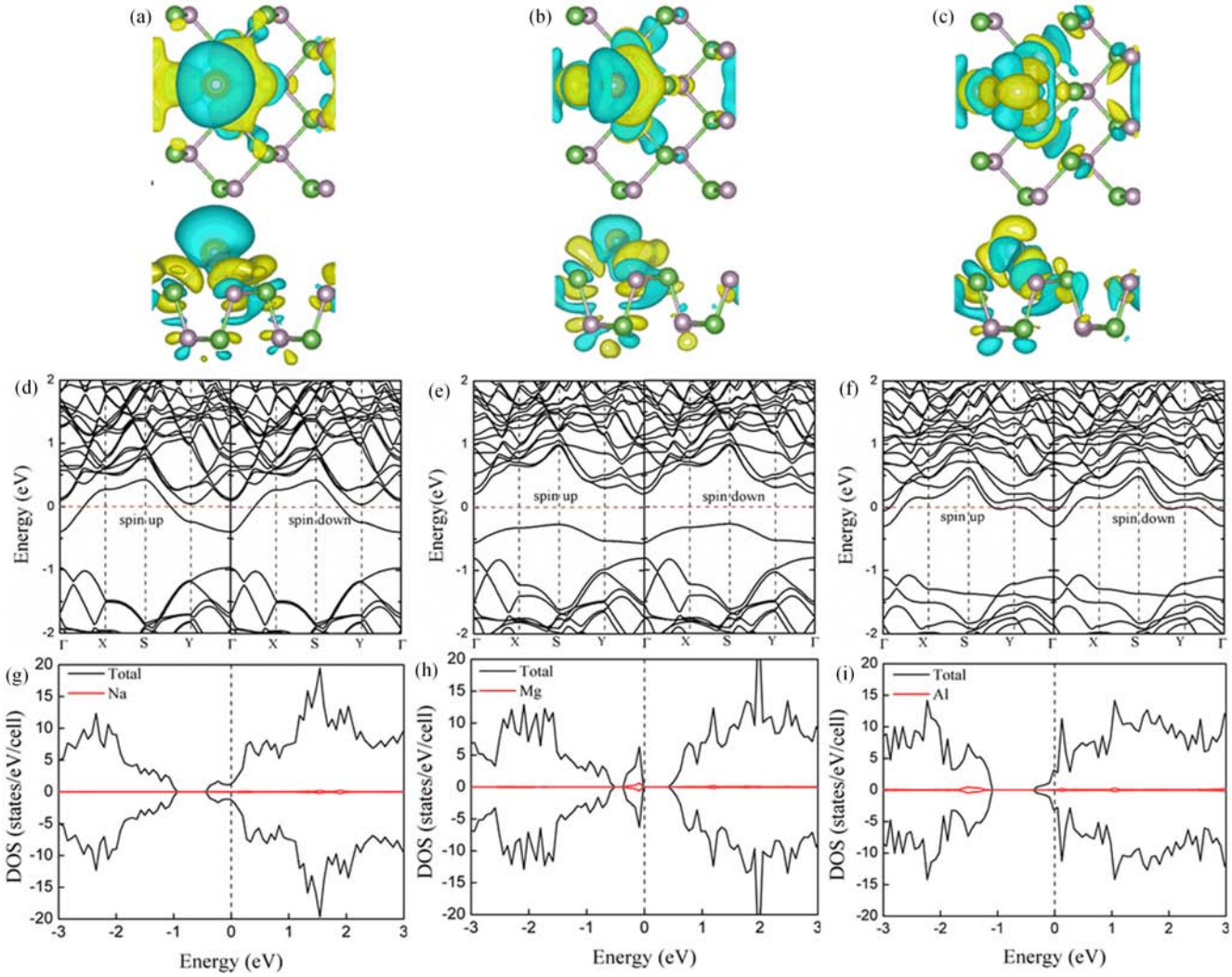

FIG. 4 The charge density difference of single (a) Na, (b) Mg, and (c) Al adsorbed on the AsP monolayer; the band structure of (d) Na-, (e) Mg-, and (f) Al-adsorbed AsP; the PDOS of (g) Na-, (h) Mg-, and (i) Al-adsorbed AsP.

C. Transition-metal (Ti, Vi, Cr, Mn, and Fe) adatoms

Afterwards, we investigated the adsorptions of 3d transition-metal atoms (Ti, V, Cr, Mn, and Fe) on AsP. The 3d transition metals (Ti, Vi, Cr, Mn, and Fe) cause diverse adsorption energies and electronic properties on AsP. All these adatoms favor the H site, forming fairly strong covalent bonds with AsP. Their adsorption energies ($E_{\rm ad}$) are −3.70, −3.11, −1.95, −2.04, and −3.14 eV for Ti, V, Cr, Mn, and Fe, respectively, which are much larger than that of TM adatoms adsorbed on graphene. The largest adsorption energy of all the adatoms is Ti atom, which has d^2 electronic configuration. The weakest interaction appears in Cr and Mn adatoms which have half-filled d-shells. Such a unique trend has also been found in TMs adsorbed carbon nanotubes [53]. To understand the charge redistribution of TMs adsorbed on AsP, the Bader charge analysis and charge density difference are made. The Bader charge analysis displays the charge of −0.97, −0.79, −0.67, −0.56, and −0.36 |e| on Ti, V, Cr, Mn, and Fe adatoms, respectively. The charge density difference of TMs adsorbed on AsP shows that the charge is accumulated in the middle region of A−P(As) bonds, as shown in FIG. 5.

FIG. 6 presents the band structures and the projected densities of states (PDOS) of TMs adsorbed system. The TM atoms tune the electronic structure of AsP thoroughly. The spin-polarized band structures appear in Ti, V, Cr, Mn and Fe adatoms adsorbed system. Therefore, all of the transition metals adsorbed on AsP under study have a magnetic moment. The total magnetic moments of TMs adsorbed systems are 2.00, 4.07, 4.98, 4.99, and 2.00 $\mu_{\rm B}$, respectively, as shown in Table I. V and Cr adsorbed on AsP present metallic behavior because that impurity bands crossed the Fermi level. While Ti, Mn and Fe adsorbed systems maintain the semiconductor property.

DOI:10.1063/1674-0068/cjcp1907136

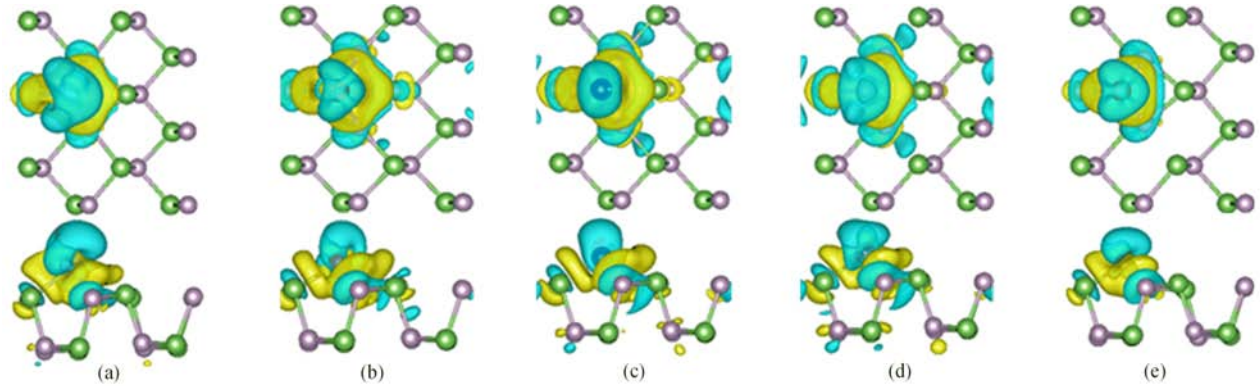

FIG. 5 The charge density difference of single (a) Ti, (b) V, (c) Cr, (d) Mn, (e) Fe adsorbed on the AsP monolayer.

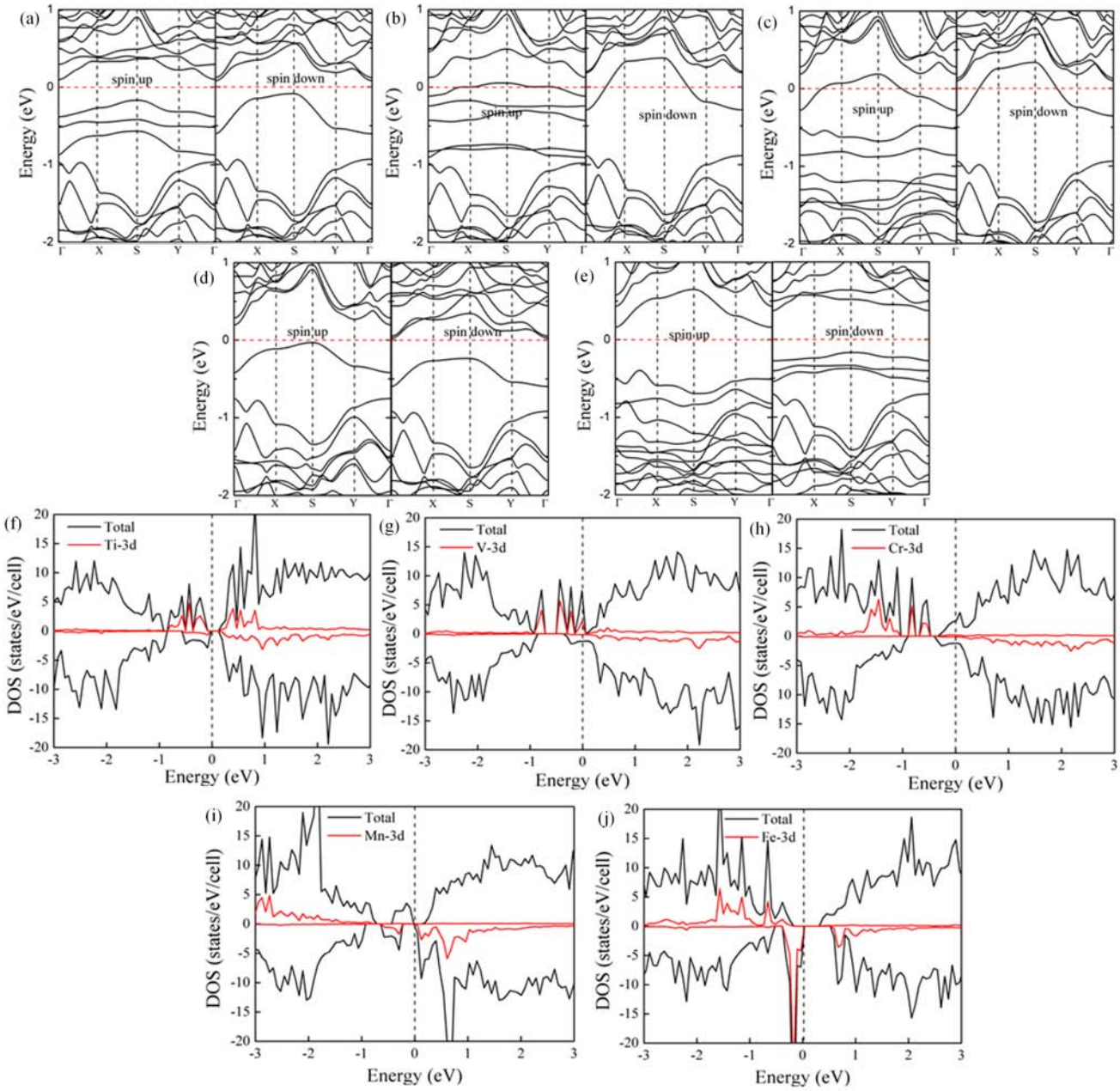

FIG. 6 The band structure of (a) Ti-, (b) V-, (c) Cr-, (d) Mn-, (e) Fe- adsorbed AsP; the PDOS of (f) Ti-, (g) V-, (h) Cr-, (i) Mn-, and (j) Fe-adsorbed AsP.

DOI:10.1063/1674-0068/cjcp1907136

The 3d states of Ti atom are mainly located in the conduction band, and mid-gap. The mid-gap of Ti peaks reduce the bandgap of Ti−AsP from 0.86 eV to 0.27 eV and 0.17 eV for spin-up and spin-down states, respectively. The 3d states of V and Cr are divided into different groups of spin states as illustrated in FIG. 6 (h) and (i), respectively. The spin-up V states are divided into four peaks and one of them dominates the region near the Fermi level. The spin-up 3d states of Cr are also divided into four peaks: two peaks appear in the valence band, and the other two peaks are in the mid-gap. For spin-down, the 3d states of V and Cr are all located in the conduction band. The 3d states of Mn and Fe are also divided into several peaks which are not across the Fermi level. The 3d states of Mn also induce mid-gap states in AsP. It is important that the up-spin top valence state exactly comes into contact with down-spin bottom conduction state at the Fermi level, as illustrated in FIG. 6(j). Thus, the Mn-adsorbed AsP changes to a bipolar spin-gapless-semiconductor [54]. The up-spin 3d states of Fe are located in the valence band and reduce bandgap to 0.56 eV. The down-spin 3d states of Fe are located in the conduction band, as well as in the mid-gap and reduce bandgap to 0.56 eV. Because of its considerable bandgap, the Fe adsorption on AsP system may be applicable in the spintronic materials.

IV. CONCLUSION

In this work, a systematic research is present on the geometry, adsorption energy, electronic and magnetic properties of 11 different adatoms adsorbed on AsP monolayer. By using spin polarized density functional theory calculations, we find that a wide variety of adsorption geometries are emerge on AsP monolayer. Most adatoms occupy the H site above the AsP monolayer except for nonmetallic adatoms. Specifically, C adatom is within the AsP monolayer plane. Electronic structures of AsP are modified by adatoms. On the AsP monolayer, Na and Al adatoms cause n-type doping without any change of the bandgap. The O atom has almost no effect on the electronic structure, while the others introduce several mid-gap states, which obviously reduce the bandgap of AsP. Among the investigated adatoms, the adsorptions of C, N, and TMs adatoms can induce relatively large magnetism in AsP monolayer. Particularly, N-, Ti- and Fe-decorated AsP become bipolar-semiconductors, while the Mn-decorated AsP becomes a bipolar spin-gapless-semiconductor. The adsorption energies of AsP are much stronger than that of graphene, BN, SiC and MoS_2. Importantly, AsP can form strong bonds with most adatoms under study while it still maintains the integrity of its structure. This research may facilitate further theoretical and experimental studies on AsP monolayer in the fields of electricity storage, nanoelectronics, as well as spintronics.

V. ACKNOWLEDGMENTS

This work was supported by the National Natural Science Foundation of China (No.11404268 and No.11774294), the Sichuan Province Applied Science and Technology Project (No.2017JY0056), and the R&D Program for International ST Cooperation and Exchanges of Sichuan province (No.2018HH0088).

[1] K. S. Novoselov, A. K. Geim, S. V. Morozov, D. Jiang, Y. Zhang, S. V. Dubonos, I. V. Grigorieva, and A. A. Firsov, Science **306**, 666 (2004).
[2] Y. Lin and J. W. Connell, Nanoscale **4**, 6908 (2012).
[3] R. T. Paine and C. K. Narula, Chem. Rev. **90**, 73 (1990).
[4] M. Xu, T. Liang, M. Shi, and H. Chen, Chem. Rev. **113**, 3766 (2013).
[5] C. Tan and H. Zhang, Chem. Soc. Rev. **44**, 2713 (2015).
[6] L. Li, Y. Yu, G. J. Ye, Q. Ge, X. Ou, H. Wu, D. Feng, X. H. Chen, and Y. Zhang, Nat. Nanotechnol. **9**, 372 (2014).
[7] H. Liu, A. T. Neal, Z. Zhu, Z. Luo, X. Xu, D. Tománek, and P. D. Ye, ACS Nano **8**, 4033 (2014).
[8] M. Buscema, D. J. Groenendijk, S. I. Blanter, G. A. Steele, H. S. J. van der Zant, and A. Castellanos-Gomez, Nano Lett. **14**, 3347 (2014).
[9] W. Lu, H. Nan, J. Hong, Y. Chen, C. Zhu, Z. Liang, X. Ma, Z. Ni, C. Jin, and Z. Zhang, Nano Res. **7**, 853 (2014).
[10] Y. Cai, G. Zhang, and Y. W. Zhang, Sci. Rep. **4**, 6677 (2014).
[11] J. Qiao, X. Kong, Z. X. Hu, F. Yang, and W. Ji, Nat. Commun. **5**, 4475 (2014).
[12] J. Xiao, M. Long, X. Zhang, J. Ouyang, H. Xu, and Y. Gao, Sci. Rep. **5**, 9961 (2015).
[13] R. Fei, A. Faghaninia, R. Soklaski, J. A. Yan, C. Lo, and L. Yang, Nano Lett. **14**, 6393 (2014).
[14] Z. Y. Ong, Y. Cai, G. Zhang, and Y. W. Zhang, J. Phys. Chem. C **118**, 25272 (2014).
[15] Y. Cai, Q. Ke, G. Zhang, Y. P. Feng, V. B. Shenoy, and Y. W. Zhang, Adv. Funct. Mater. **25**, 2230 (2015).
[16] Y. Du, H. Liu, Y. Deng, and P. D. Ye, ACS Nano **8**, 10035 (2014).
[17] J. Na, Y. T. Lee, J. A. Lim, D. K. Hwang, G. T. Kim, W. K. Choi, and Y. W. Song, ACS Nano **8**, 11753 (2014).
[18] A. Avsar, I. J. Vera-Marun, J. Y. Tan, K. Watanabe, T. Taniguchi, A. H. Castro Neto, and B. Özyilmaz, ACS Nano **9**, 4138 (2015).
[19] W. Zhu, M. N. Yogeesh, S. Yang, S. H. Aldave, J. S. Kim, S. Sonde, L. Tao, N. Lu, and D. Akinwande, Nano Lett. **15**, 1883 (2015).
[20] P. J. Jeon, Y. T. Lee, J. Y. Lim, J. S. Kim, D. K. Hwang, and S. Im, Nano Lett. **16**, 1293 (2016).
[21] M. V. Kamalakar, B. Madhushankar, A. Dankert, and S. P. Dash, Small **11**, 2209 (2015).

DOI:10.1063/1674-0068/cjcp1907136

[22] S. Zhao, W. Kang, and J. Xue, J. Mater. Chem. A **2**, 19046 (2014).
[23] W. Li, Y. Yang, G. Zhang, and Y. W. Zhang, Nano Lett. **15**, 1691 (2015).
[24] J. Sun, H. W. Lee, M. Pasta, H. Yuan, G. Zheng, Y. Sun, Y. Li, and Y. Cui, Nat. Nanotechnol. **10**, 980 (2015).
[25] R. Babar and M. Kabir, J. Phys. Chem. C **120**, 14991 (2016).
[26] L. Zu, X. Gao, H. Lian, C. Li, Q. Liang, Y. Liang, X. Cui, Y. Liu, X. Wang, and X. Cui, J. Alloy. Compd. **770**, 26 (2019).
[27] Y. Cai, Q. Ke, G. Zhang, and Y. W. Zhang, J. Phys. Chem. C **119**, 3102 (2015).
[28] A. N. Abbas, B. Liu, L. Chen, Y. Ma, S. Cong, N. Aroonyadet, M. Köpf, T. Nilges, and C. Zhou, ACS Nano **9**, 5618 (2015).
[29] S. Cui, H. Pu, S. A. Wells, Z. Wen, S. Mao, J. Chang, M. C. Hersam, and J. Chen, Nat. Commun. **6**, 8632 (2015).
[30] B. Liu, M. Köpf, A. N. Abbas, X. Wang, Q. Guo, Y. Jia, F. Xia, R. Weihrich, F. Bachhuber, and F. Pielnhofer, Adv. Mater. **27**, 4423 (2015).
[31] Z. Zhu, J. Guan, and D. Tománek, Nano Lett. **15**, 6042 (2015).
[32] F. Shojaei and H. S. Kang, J. Phys. Chem. C **119**, 20210 (2015).
[33] M. Xie, S. Zhang, B. Cai, Y. Huang, Y. Zou, B. Guo, Y. Gu, and H. Zeng, Nano Energy **28**, 433 (2016).
[34] X. Wang, K. Maeda, A. Thomas, K. Takanabe, G. Xin, J. M. Carlsson, K. Domen, and M. Antonietti, Nat. Mater. **8**, 76 (2008).
[35] C. Cao, M. Wu, J. Jiang, and H. P. Cheng, Phys. Rev. B **81**, 205424 (2010).
[36] M. Wu, C. Cao, and J. Z. Jiang, Nanotechnology **21**, 505202 (2010).
[37] X. Lin and J. Ni, Phys. Rev. B **86**, 075440 (2012).
[38] H. Sahin and F. M. Peeters, Phys. Rev. B **87**, 085423 (2013).
[39] J. Sivek, H. Sahin, B. Partoens, and F. M. Peeters, Phys. Rev. B **87**, 085444 (2013).
[40] V. Q. Bui, T. T. Pham, H. V. S. Nguyen, and H. M. Le, J. Phys. Chem. C **117**, 23364 (2013).
[41] T. P. Kaloni, J. Phys. Chem. C **118**, 25200 (2014).
[42] S. S. Li, C. W. Zhang, W. X. Ji, F. Li, P. J. Wang, S. J. Hu, S. S. Yan, and Y. S. Liu, Phys. Chem. Chem. Phys. **16**, 15968 (2014).
[43] G. Kresse and J. Furthmüller, Comput. Mater. Sci. **6**, 15 (1996).
[44] G. Kresse and J. Furthmüller, Phys. Rev. B **54**, 11169 (1996).
[45] J. P. Perdew, K. Burke, and M. Ernzerhof, Phys. Rev. Lett. **77**, 3865 (1996).
[46] P. E. Blöchl, Phys. Rev. B **50**, 17953 (1994).
[47] S. Grimme, J. Comput. Chem. **27**, 1787 (2006).
[48] B. Cordero, V. Gómez, A. E. Platero-Prats, M. Revés, J. Echeverra, E. Cremades, F. Barragán, and S. Alvarez, Dalton Trans. 2832 (2008).
[49] B. Gamoke, D. Neff, and J. Simons, J. Phys. Chem. A **113**, 5677 (2009).
[50] D. Pan, S. Wang, B. Zhao, M. Wu, H. Zhang, Y. Wang, and Z. Jiao, Chem. Mater. **21**, 3136 (2009).
[51] H. Wang, C. Zhang, Z. Liu, L. Wang, P. Han, H. Xu, K. Zhang, S. Dong, J. Yao, and G. Cui, J. Mater. Chem. **21**, 5430 (2011).
[52] W. Yuan, Y. Zhou, Y. Li, C. Li, H. Peng, J. Zhang, Z. Liu, L. Dai, and G. Shi, Sci. Rep. **3**, 2248 (2013).
[53] E. Durgun, S. Dag, S. Ciraci, and O. Gülseren, J. Phys. Chem. B **108**, 575 (2004).
[54] Y. Li, Z. Zhou, P. Shen, and Z. Chen, ACS Nano **3**, 1952 (2009).

DOI:10.1063/1674-0068/cjcp1907136